Femtosecond-resolution longitudinal bunch profile monitor

using coherent transition radiation imaging

September 1st, 2026

15th International Beam Instrumentation Conference - IBIC 2026

Ana Guisao-Betancur[1,2], Joseph Wolfenden[1,2], Erik Mansten[3], Sara Thorin[3], Johan Lundquist[4], Oliver Grimm[3], Carsten Welsch[1,2]

A.M.Guisao-Betancur@liverpool.ac.uk

[1]. Department of Physics, University of Liverpool, Liverpool L69 7ZX, UK

[2]. Cockcroft Institute, Sci-Tech Daresbury, Daresbury WA4 4AD, UK

[3]. MAX IV Laboratory, Lund University, Lund 224 84, Sweden

[4]. Department of Physics, Lund University, Lund 223 64, Sweden

Content overview

1. Problem description
2. Transition radiation-based monitor
3. Designing the bunch profile monitor
4. CTR image acquisition and analysis
5. Longitudinal profile reconstruction
6. Discussion and conclusions

A.M.Guisao-Betancur@liverpool.ac.uk

1. Problem description

A.M.Guisao-Betancur@liverpool.ac.uk

1. Problem description

Need for monitoring ultrashort electron bunches in the femtosecond range

Longitudinal diagnostics in short-pulse accelerators ⟹ Challenge of measuring fs-range bunches

Example: plasma-based accelerators can produce **ultra-short electron bunches** and impart **energy gain of several GeV** in accelerating distances of only few centimetres.

Figure 1. Wakefield generation and electron beam acceleration in a plasma accelerator showing the behaviour in a laser-driven plasma (wakefield) accelerator (LWFA)* .

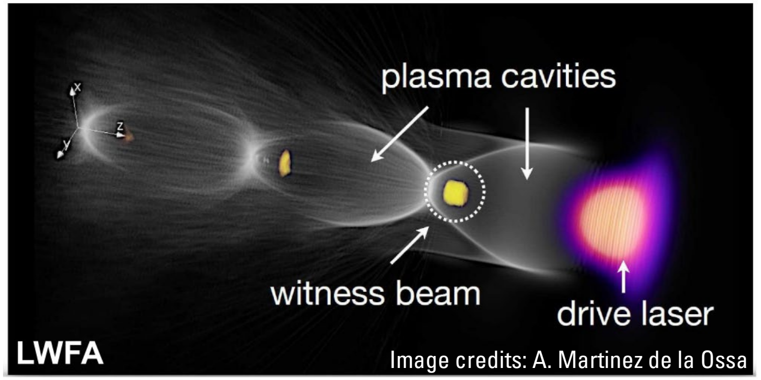

In the case of **EuPRAXIA** and **other short-pulse accelerators**, bunch lengths can be **sub-fs to a few hundreds of fs** long. This brings a **challenge** for the development of longitudinal diagnostics.

Table 1. Summary of the electron beam properties for EuPRAXIA (at entrance of undulator for FEL)*.

Parameter	Range of exploration
Bunch length (FWHM)	< 30 fs
Energy	$1 - 5$ GeV
Bunch charge	$5 - 100$ pC
Repetition rate	$20 - 100$ Hz
Normalised emittance	≤ 1 mm mrad
Energy spread	< 1 %

*Assmann, R. W. et al. EuPRAXIA Conceptual Design Report.

1. Problem description

Measuring ultrashort electron bunch profiles

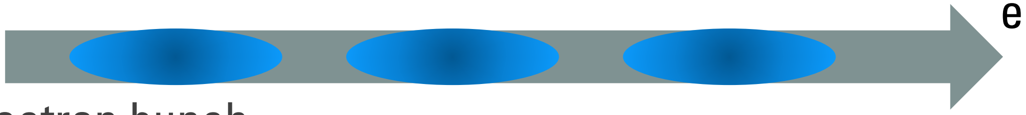

Electron beam
e-beam

Electron bunch
e-bunch

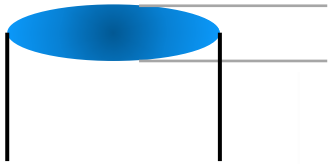

Bunch transverse size

Bunch length

Transverse deflecting structures are considered the gold standard for length measurements.

Demonstrated **time resolutions** in the sub- to few-fs "ultrashort" ranges.

Costly to produce and operate.

Destructive and invasive, not suitable at intermediate acc. stages.

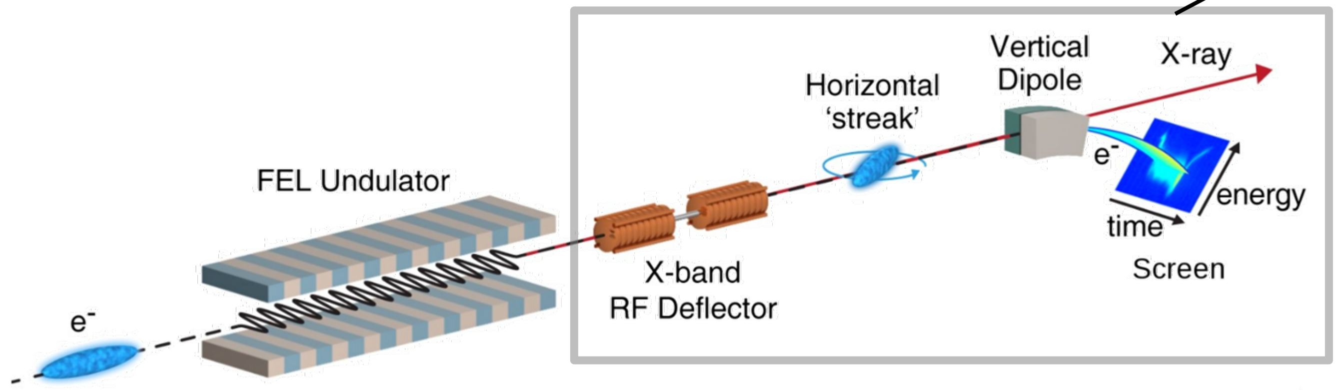

Figure 2. Schematic of an example X-band Transverse Deflecting Cavity (TDC)*.

*SLAC SCLS (Stanford) Documentation.

Objective

Develop a **cost-effective**, **minimally-invasive** and **small footprint** alternative diagnostic.

A.M.Guisao-Betancur@liverpool.ac.uk

2. Transition radiation-based monitor

A.M.Guisao-Betancur@liverpool.ac.uk

2. Transition radiation-based monitor

About generation of (coherent) transition radiation

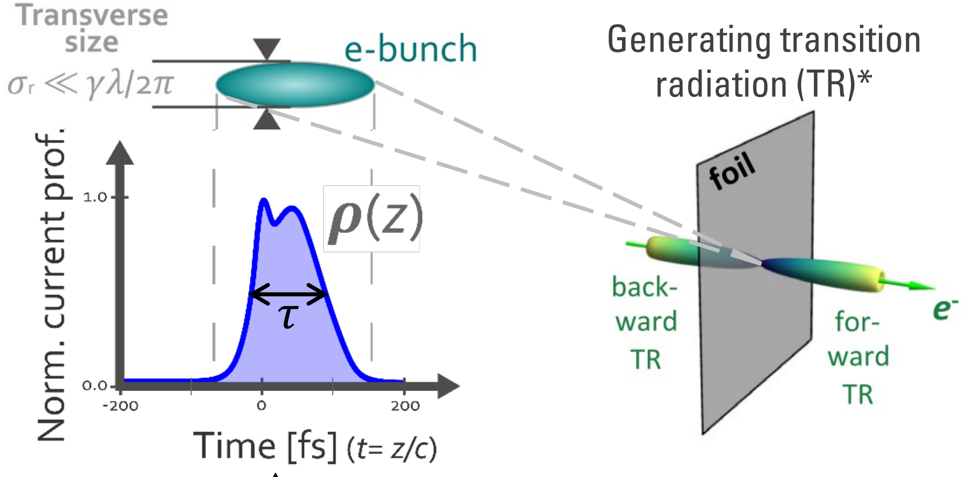

Used to reconstruct the profile.

Limited by:
- The missing phase.
- The frequency cut-offs.

1. It is typically **broadband** and it is **coherent** (CTR) for $\lambda \geq c \cdot \tau$ **

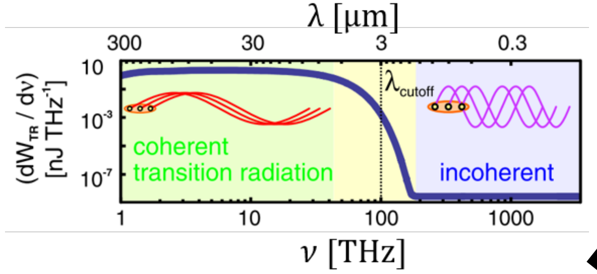

Can be measured directly with spectrometry.

$$F(\mathbf{k}) = F_{\mathrm{trans}}(\mathbf{k}_r) F_{\mathrm{long}}(\mathbf{k}_z)$$

Transverse coherence =1

Longitudinal form factor

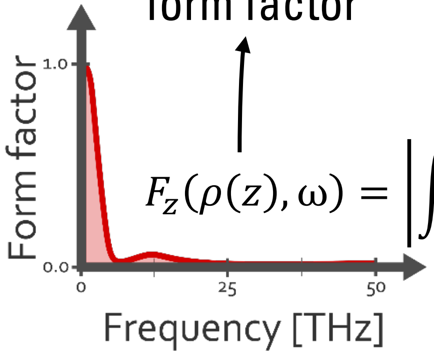

$$F_z(\rho(z), \omega) = \left| \int_{-\infty}^{\infty} \boldsymbol{\rho}(\boldsymbol{z}) e^{-i\frac{\omega}{c}z} dz \right|^2 = |\widetilde{\boldsymbol{\rho}}(\boldsymbol{\omega})|^2$$

2. The **spatial distribution** of the source of TR **depends on λ***

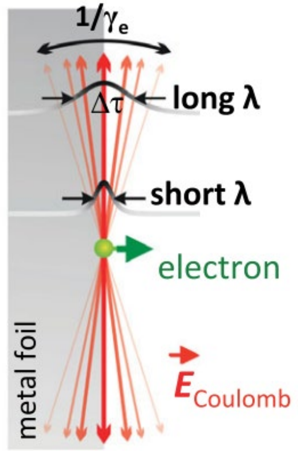

Proposing:
measuring indirectly with broadband imaging of this source distribution.

*M. C. Downer, et. al. Diagnostics for plasma-based electron accelerators.
**O. Zarini, et. al. Multioctave high-dynamic range optical spectrometer for single-pulse, longitudinal characterization of ultrashort electron bunches.

3. Designing the bunch profile monitor

A.M.Guisao-Betancur@liverpool.ac.uk

3. Designing the bunch profile monitor

Identifying the requirements for the MAX IV short pulse facility (SPF)

Figure 3. Accelerator layout at MAX IV, Lund, Sweden*.

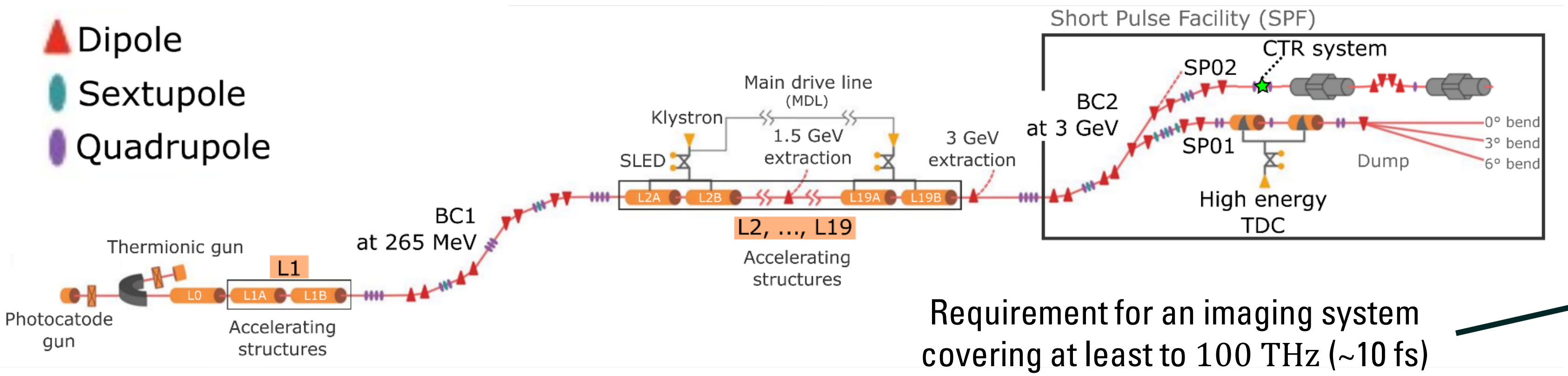

Requirement for an imaging system covering at least to 100 THz (~10 fs)

$$\boldsymbol{\lambda \gtrsim 3\ \mu m}$$

Transverse coherence condition $\sigma_r \ll \gamma\lambda/2\pi$

$\gamma\lambda/2\pi \approx$ **2800 μm** at 3 μm ✓

Table 2. Electron beam parameters at the SPF (and CTR location).

Parameter	Value / range
Bunch length (FWHM)	10 – 100 fs
RMS transverse size	few 100 μm
Energy	3 GeV
Bunch charge	≈ 100 pC
Repetition rate	10 Hz
Normalised emittance	≈ 2 mm mrad
Energy spread	< 0.1 %

*Guisao-Betancur, A. et al. Designing a Femtosecond-Resolution Bunch Length Monitor Using Coherent Transition Radiation Images.

3. Designing the bunch profile monitor

Material considerations in the THz range

Transmission of materials **needed for the viewing window**, as well as for the use of lenses and other transmissive elements.

$\boldsymbol{\lambda \gtrsim 3\mu m}$ (~10fs)

HDPE: High-density polyethylene.
TPX: Polymethylpentene.

Polymers*

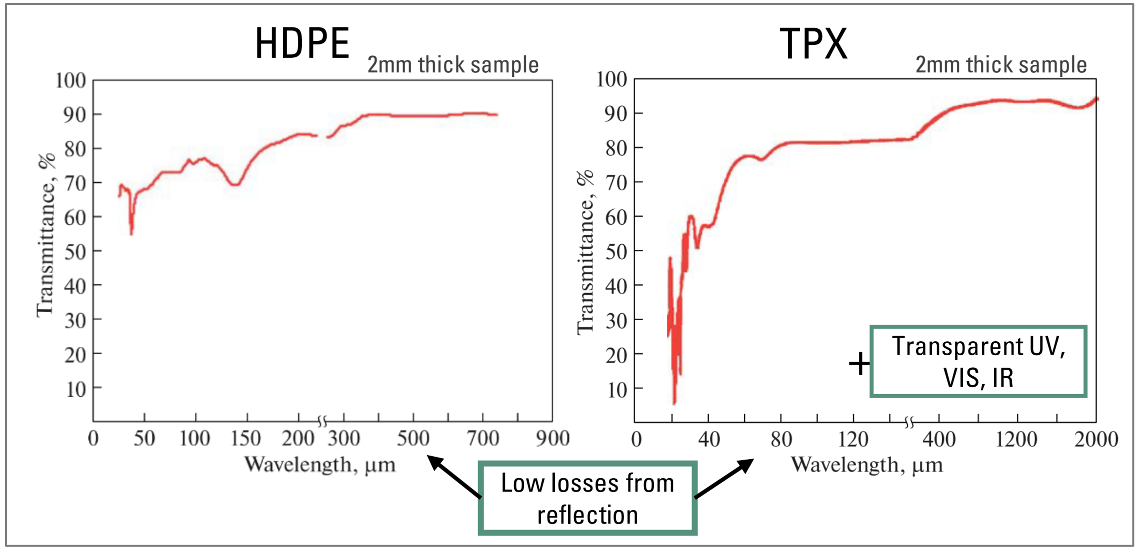

CQ: Crystalline Quartz.
HRFZ-Si: High-Resistance Float Zone Silicon.
PD: Polycrystalline Diamond.

Crystals*

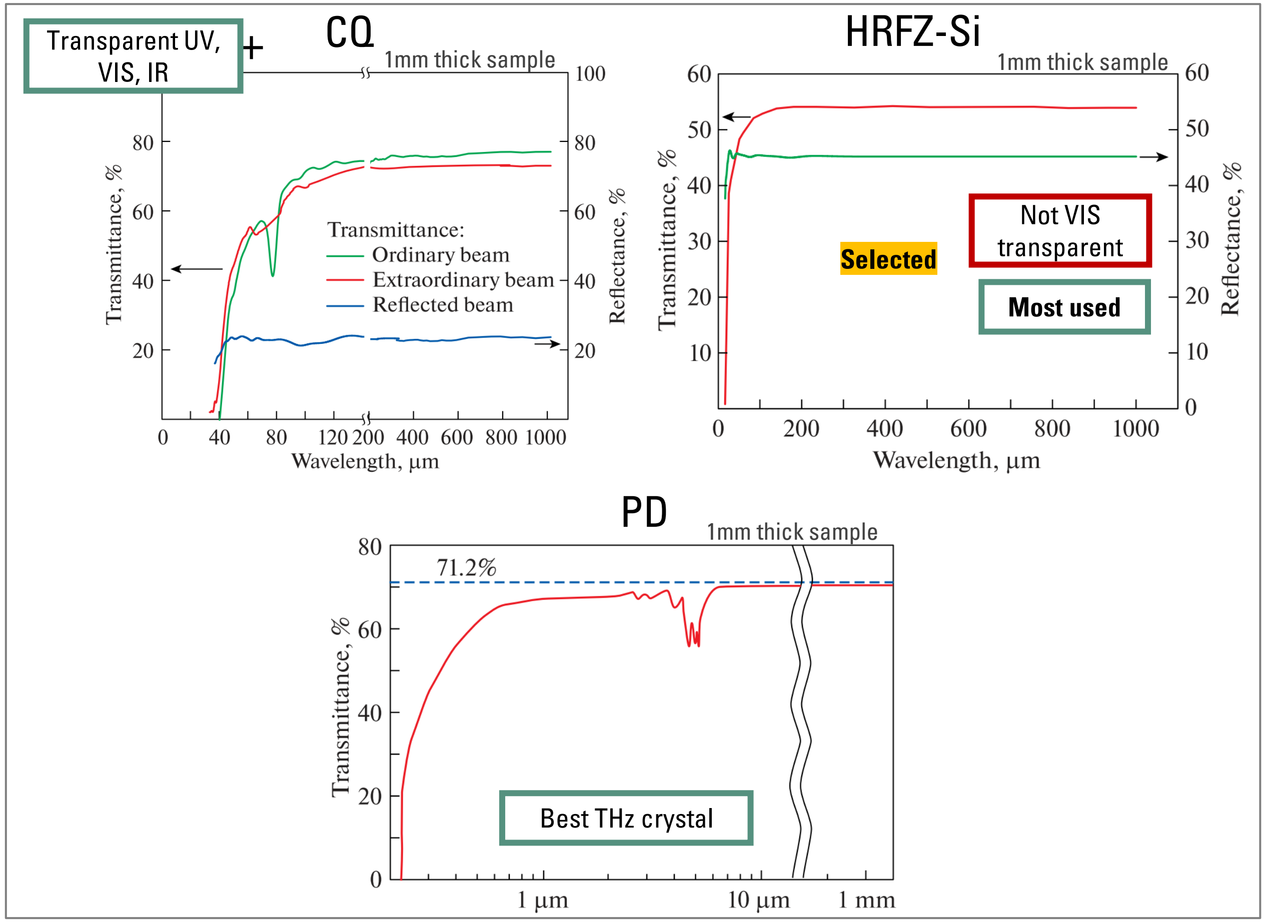

*V. Rogalin, et. al. Optical Materials for the THz Range.

3. Designing the bunch profile monitor

Final iteration: 2x magnification with OAP mirrors

Figure 6. OAP imaging system.

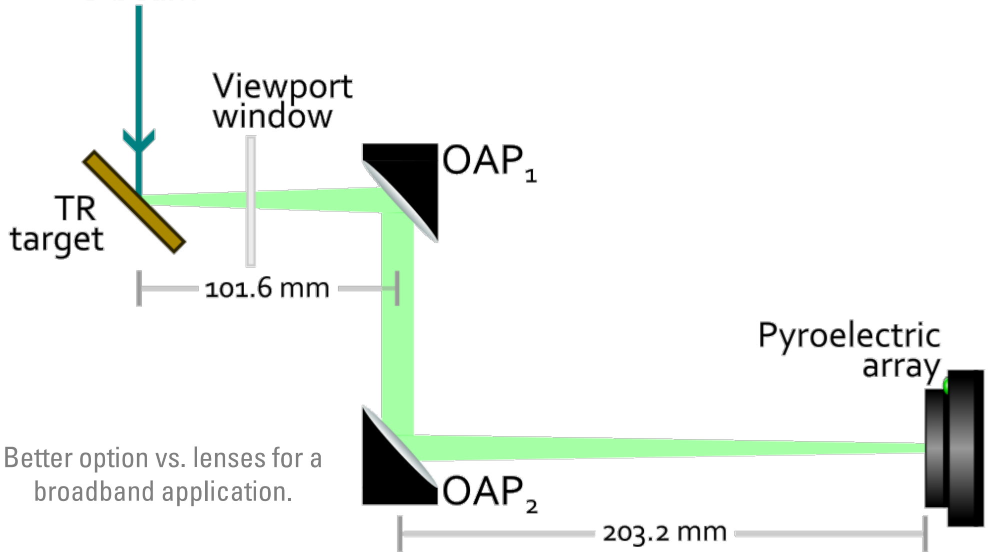

Better option vs. lenses for a broadband application.

Geometric aberrations but can be used as features for the measurements.

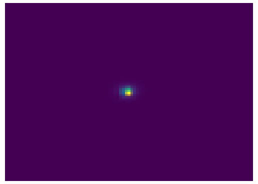

Materials

- Viewport: High Resistivity Float Zone Silicon (HRFZ-Si).
- Off-Axis Parabolic mirrors: Protected Silver (Thorlabs).
- Pyroelectric Array: Pyrocam™ IIIHR GigE.

Figure 7. Optical properties for the elements on the OAP imaging system*.

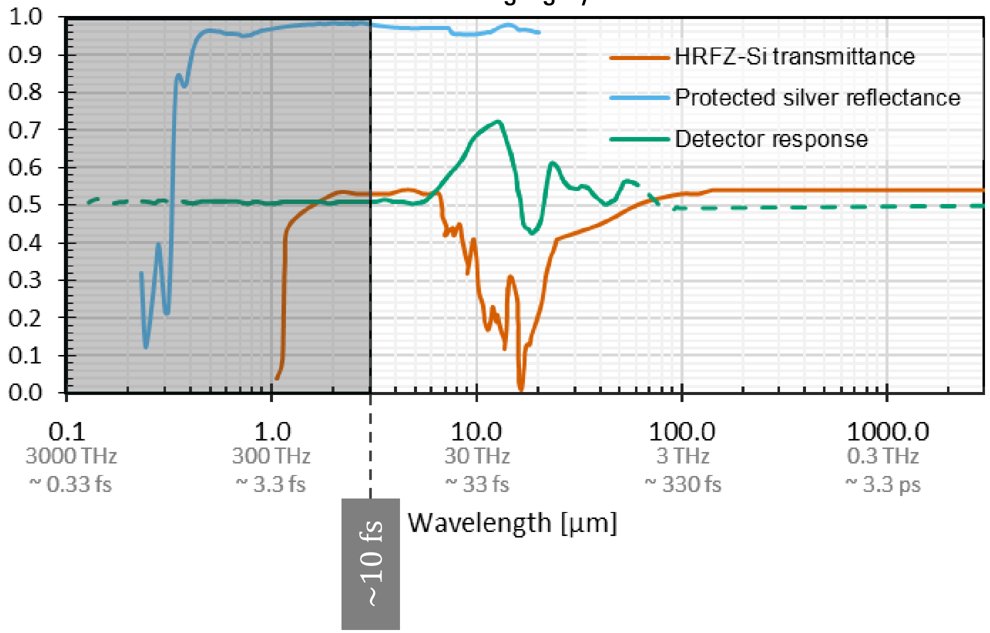

*Guisao-Betancur, A. et al. Designing a Femtosecond-Resolution Bunch Length Monitor Using Coherent Transition Radiation Images.

4. CTR image acquisition and analysis

A.M.Guisao-Betancur@liverpool.ac.uk

4. CTR image acquisition and analysis

CTR spatial distribution image simulation and relation to the longitudinal bunch profile

Figure 8. CTR image production.

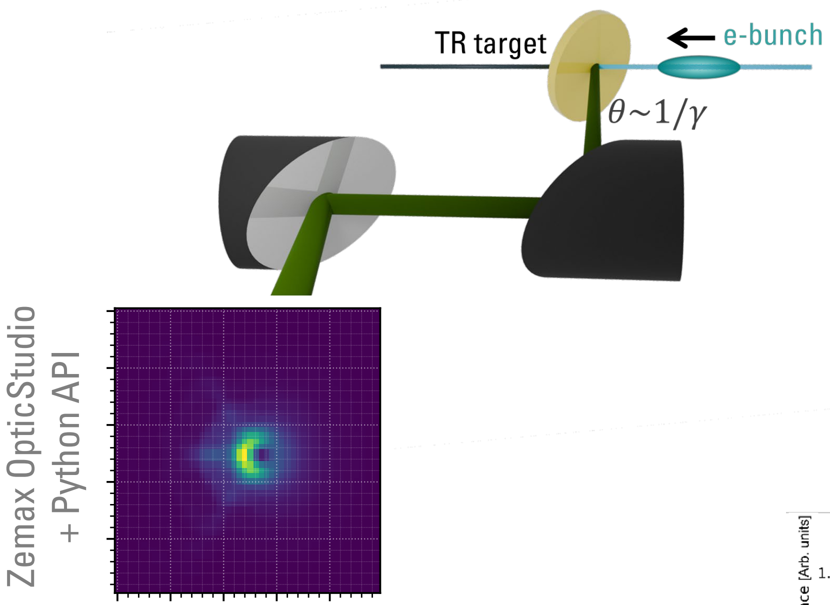

Point-to-point spatial image distribution for an e-bunch

Detection bandwidth

Modulation from the detector $\boldsymbol{D(\omega)}$ and optical components $\boldsymbol{T(\omega)}$

$$\frac{dI^i_{bunch}}{dr} \approx N_e^2 \int_{\Delta\omega} \frac{d^2 I^i_e}{d\omega dr} F_z(\rho(z),\omega) D(\omega)\, T(\omega)\, d\omega$$

Normalising the image

Single electron spectral images

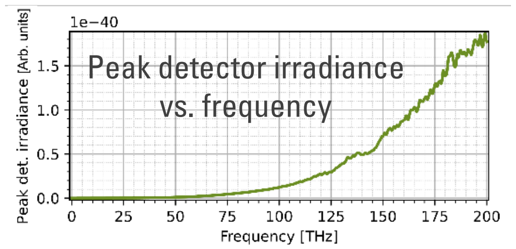

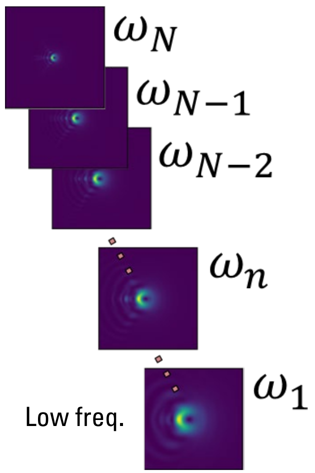

Longitudinal form factor

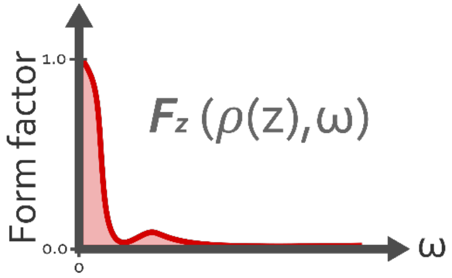

Wolfenden, J. et al. Coherent Transition Radiation Spatial Imaging As a Bunch Length Monitor.
Shkvarunets, A. G. & Fiorito, R. B. Vector electromagnetic theory of transition and diffraction radiation with application to the measurement of longitudinal bunch size.

A.M.Guisao-Betancur@liverpool.ac.uk

4. CTR image acquisition and analysis

Direct analysis of CTR images

Figure 9. Methodology for CTR image analysis*.

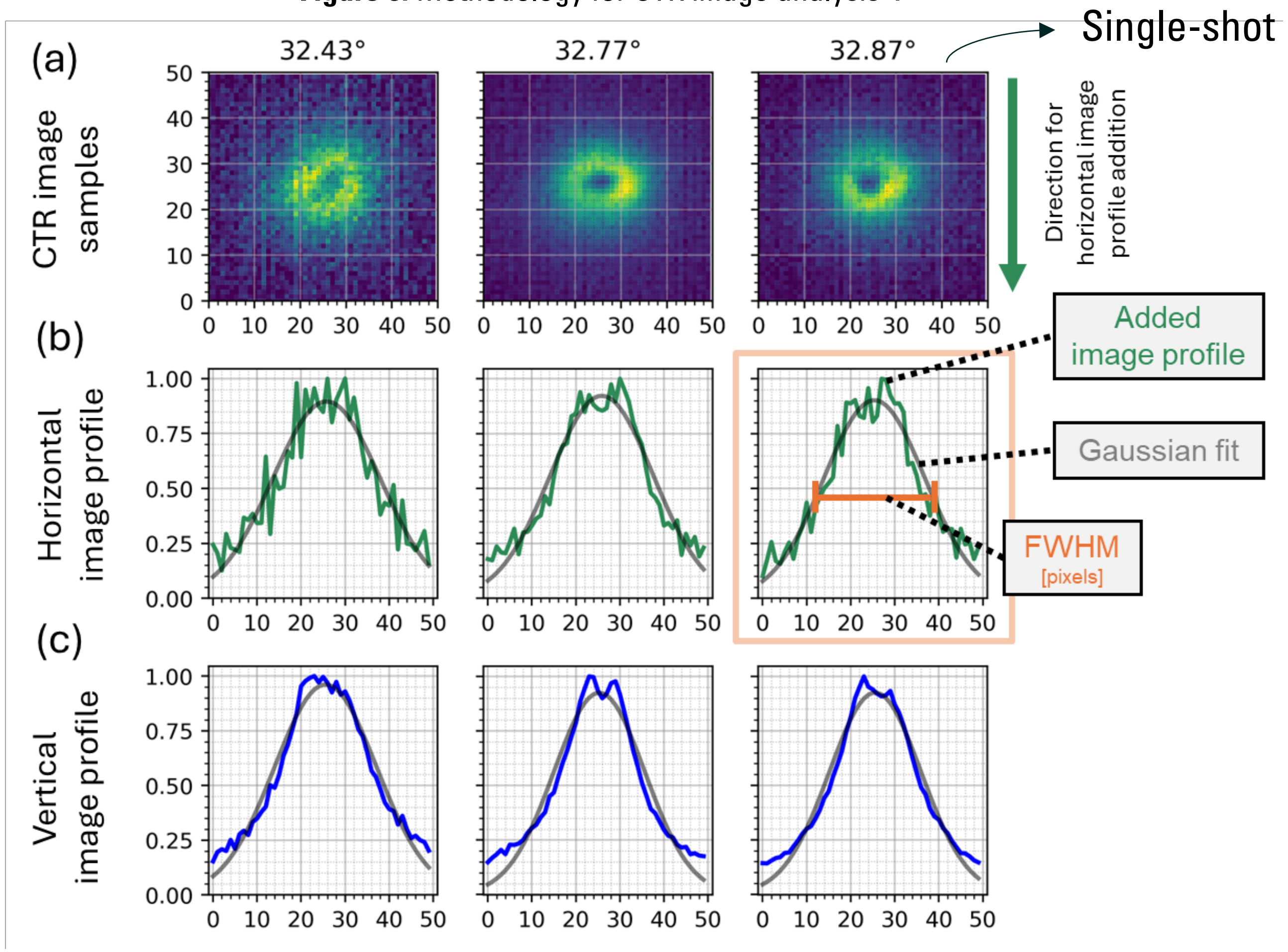

(a) **Examples of CTR images** to be analysed.

(b) Horizontal **image profiles** obtained by summing pixel values vertically, fitted to Gaussians, and FWHM **extracted.**

(c) Vertical image profiles.

The same can be done for other features: $\sqrt{m^2}$, σ, skewness, kurtosis, etc.

*Guisao-Betancur, A. et al. Designing a Femtosecond-Resolution Bunch Length Monitor Using Coherent Transition Radiation Images.

4. CTR image acquisition and analysis

Analysis of simulated CTR images from idealised profiles

Figure 10. Analysis of simulated Gaussian profiles*.

(a) Gaussians

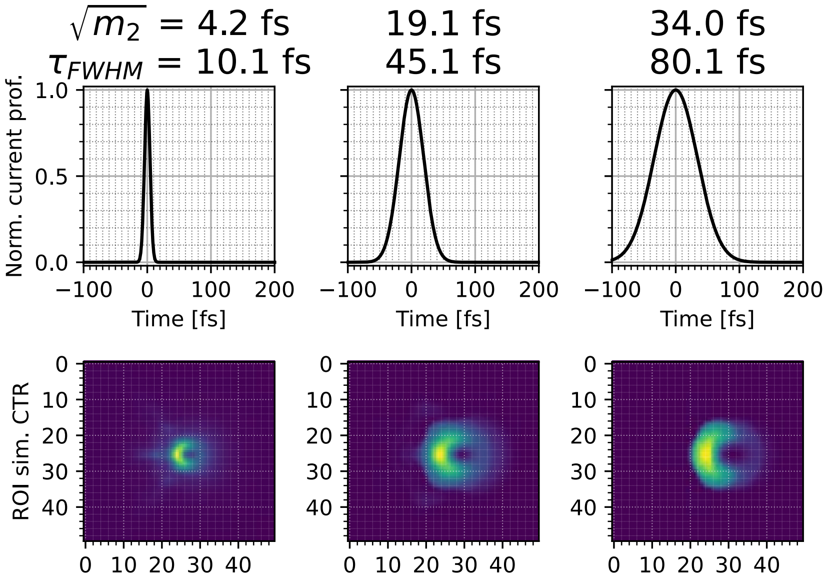

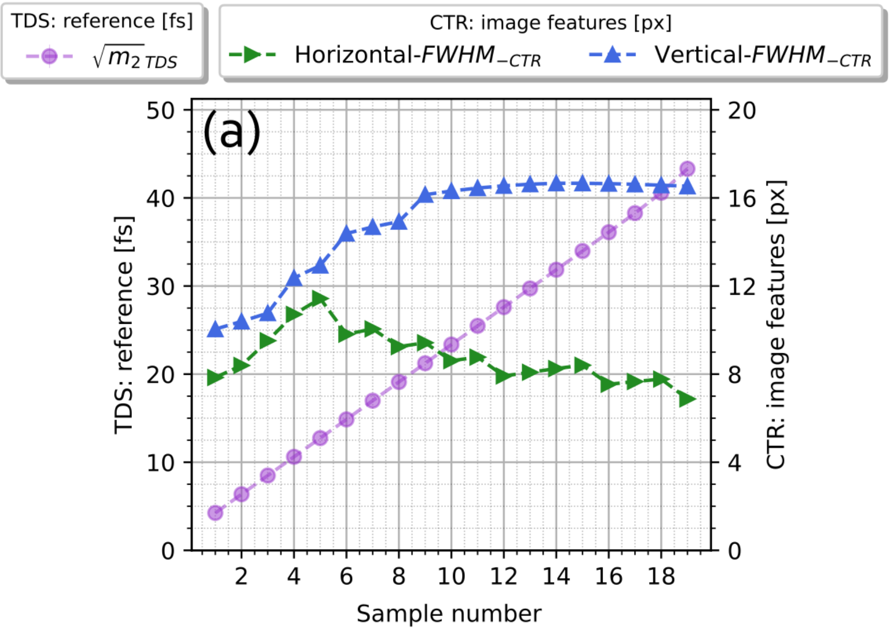

- Steady growth of the CTR image.

*Guisao-Betancur, A. et al. Studying Coherent Transition Radiation Spatial Image Features for Bunch Length Diagnostics.

4. CTR image acquisition and analysis

Analysis of simulated CTR images from idealised profiles

Figure 11. Analysis of simulated Gaussian profiles with high frequency features*.

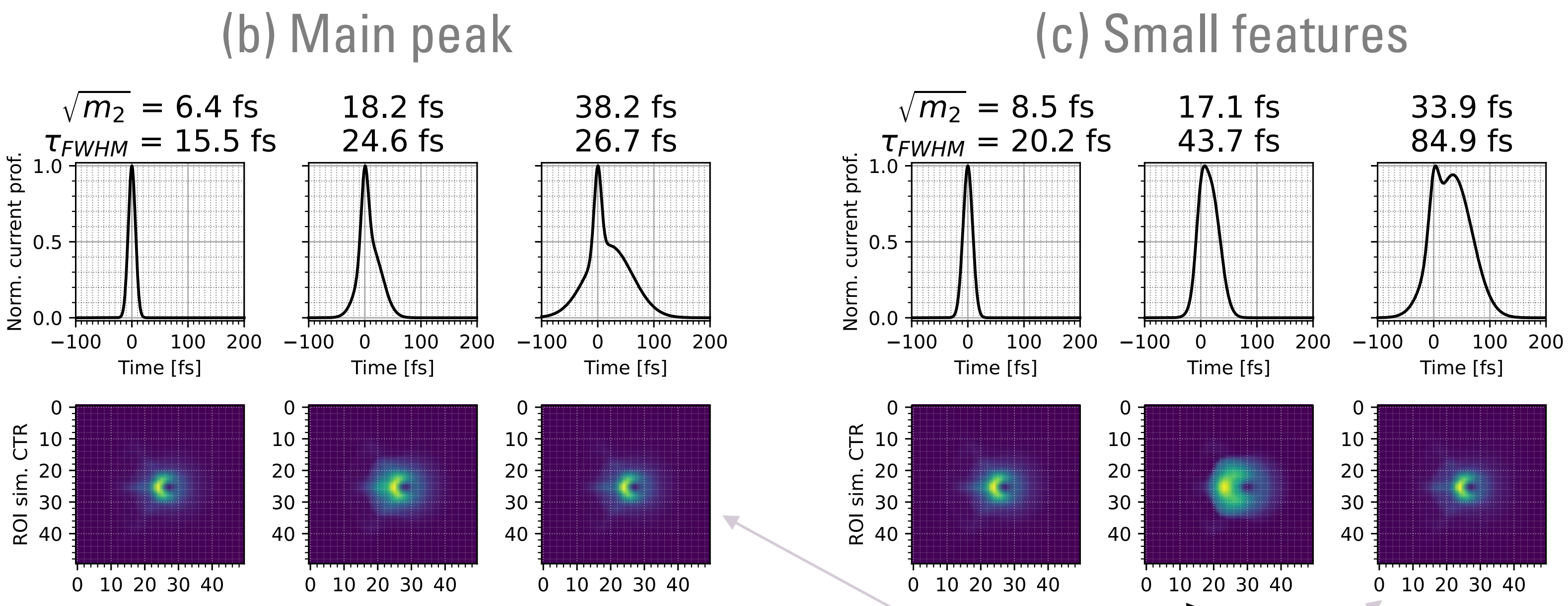

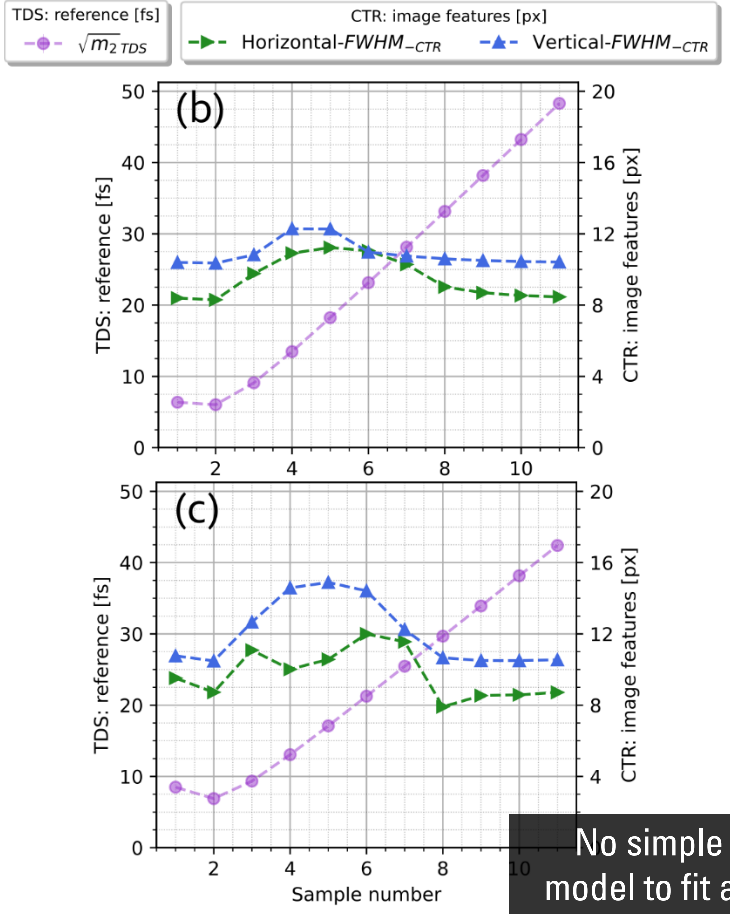

› CTR image grows when the spectral intensities of the lower freqs. of the secondary bunch are comparable to the high freqs. of the peak.

› Eventually the high frequencies of the peak become dominant, effectively "shrinking" the CTR image visible area.

No simple model to fit all cases

*Guisao-Betancur, A. et al. Studying Coherent Transition Radiation Spatial Image Features for Bunch Length Diagnostics.

4. CTR image acquisition and analysis

Data acquisition on site

Figure 12. Parameter scan locations at MAX IV, Lund, Sweden.

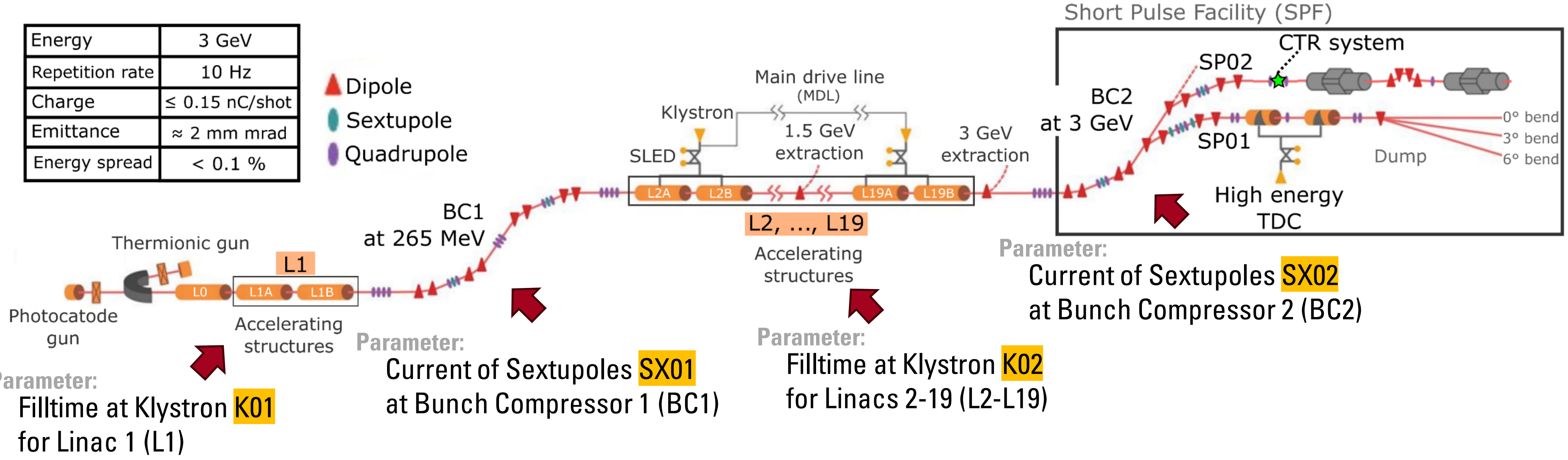

Beamtime	Date	Scanned parameters
Installation + data	03/2025	K01, K02, SX01, SX02
Data	03/2026	K01, SX01
Data	05/2026	K01, SX01

A.M.Guisao-Betancur@liverpool.ac.uk

4. CTR image acquisition and analysis

Monitor installation and data collection

Figure 13. SPF data collection positions.

CTR monitor location

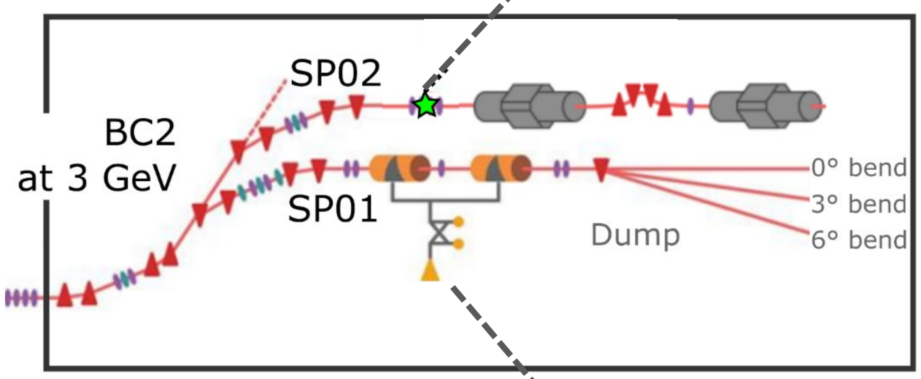

Transverse deflecting cavity (TDC)
for reference measurements

Figure 14. CTR imaging system installation.

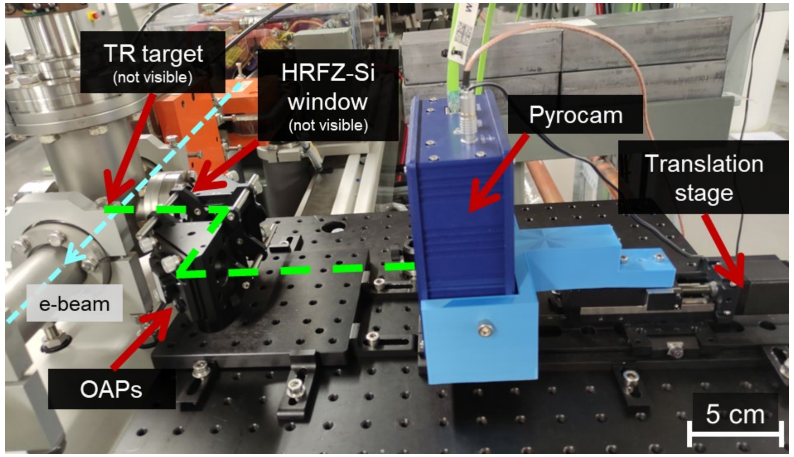

Filltime @ K01

CTR

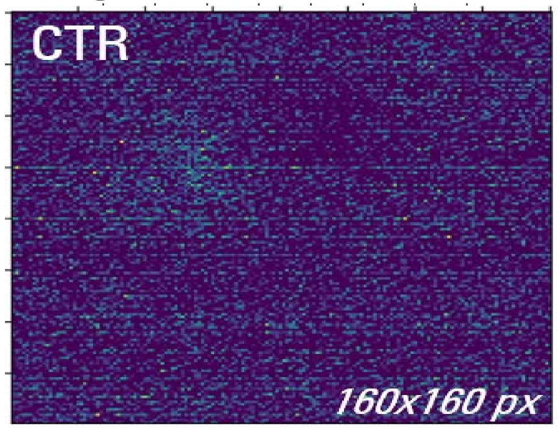

TDC

160x160 px

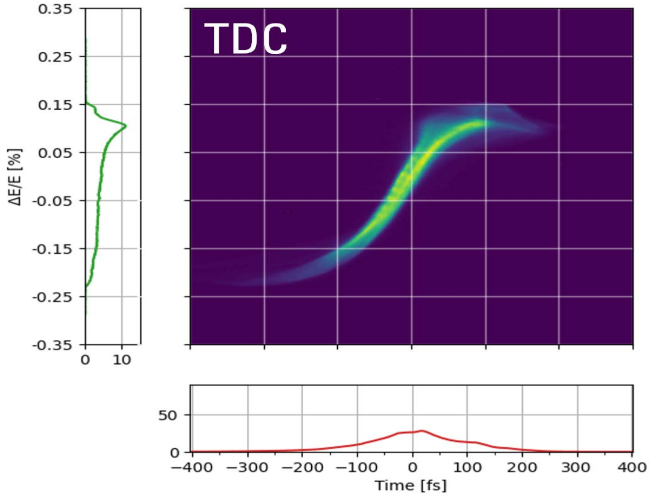

4. CTR image acquisition and analysis

Analysis of experimental CTR images

Figure 15. Analysis for a 1D current scan at bunch compressor (BC1).

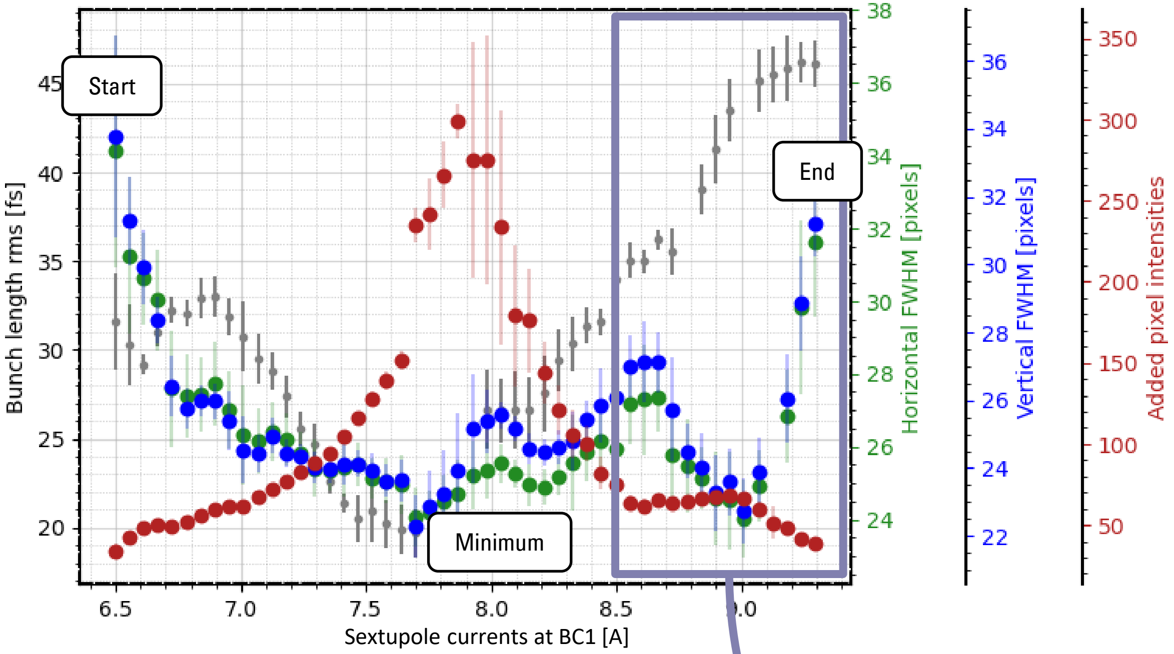

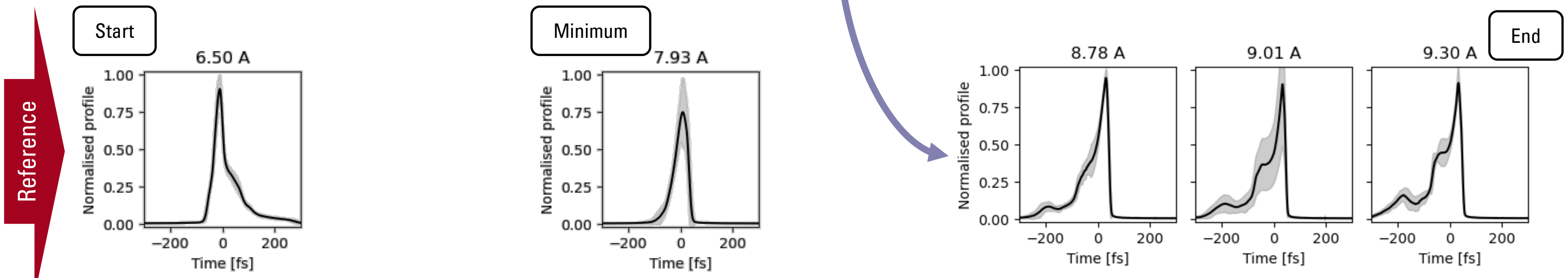

The CTR image picks up more detail from the electron bunch, such as sharp and small structures, not only the length.

Realistically, too complex for direct analysis ⟹

Proposing:
use of deep learning for the study of the image features and bunch profile reconstruction.

5. Longitudinal profile reconstruction

A.M.Guisao-Betancur@liverpool.ac.uk

5. Longitudinal profile reconstruction

Ensemble models for bunch profile reconstruction

Figure 16. Convolutional Neural Network schematic for bunch profile reconstruction from a single CTR image.

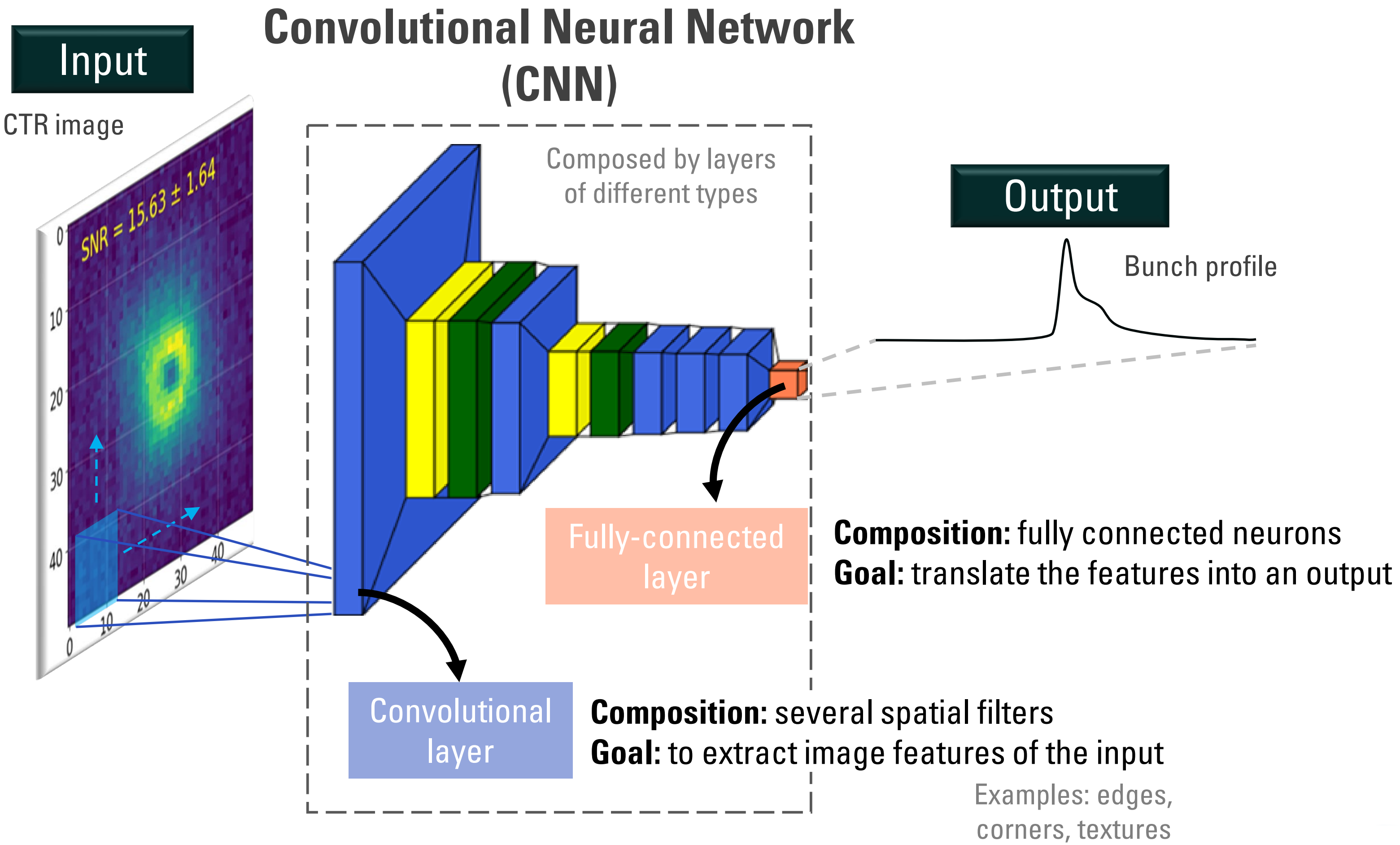

Figure 17. Schematic of CNN ensemble model.

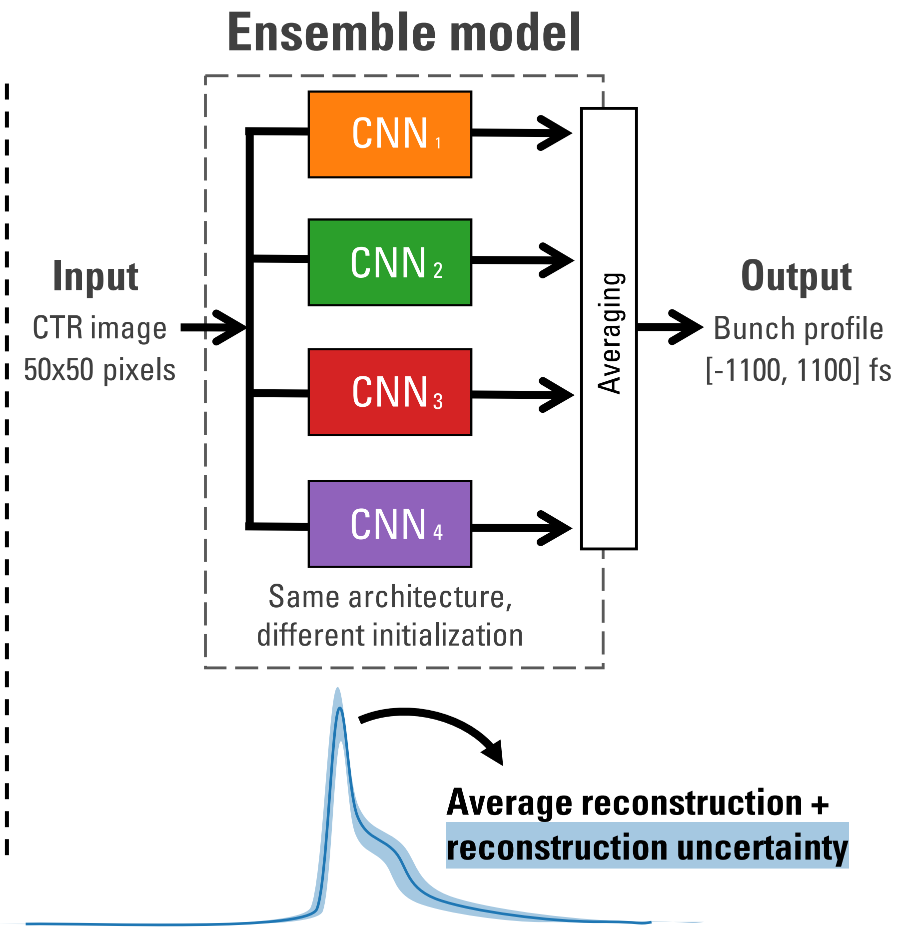

5. Longitudinal profile reconstruction

Reconstruction results

Figure 18. Examples of reconstructed bunch profiles from experimental measurements at MAX IV.

Input

CTR image
50x50 pixels

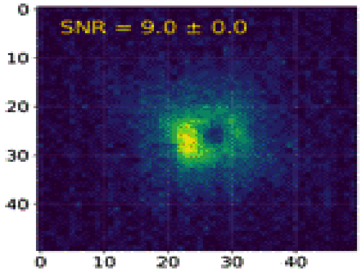

Ensemble model

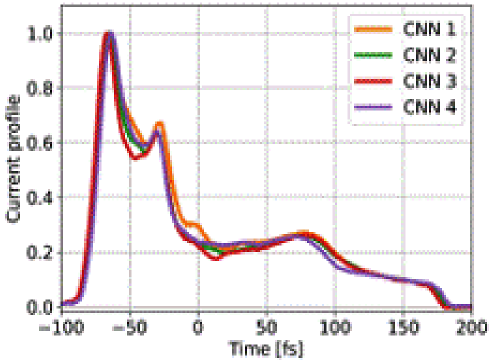

Output

Bunch profile

4001 long array
[-1100, 1100] fs

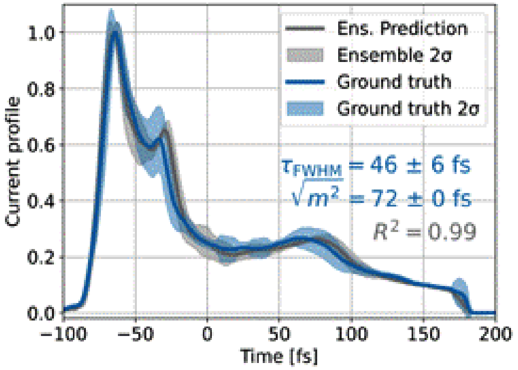

Phase 1: Pre-processing

- CTR experimental images
- TDC reference benchmark data

} Same machine parameters, taken with some time difference.

Phase 2: Training/testing experiments

i. Single-shot mode:

1 shot out of the 20 at random

ii. Single-shot mode but **multi-shot statistics**:

use all 20 shots in single-shot mode and then average

5. Longitudinal profile reconstruction

Phase 1: Pre-processing of TDC profiles and CTR images

The phase of the original profile can't be recovered from the form factor, so the reconstructions are not unique in general.

$$\sqrt{F_z} = |\tilde{\rho}(\omega)| \neq |\tilde{\rho}(\omega)| e^{i\phi(\omega)}$$

Figure 19. Head-tail orientation and image generation.

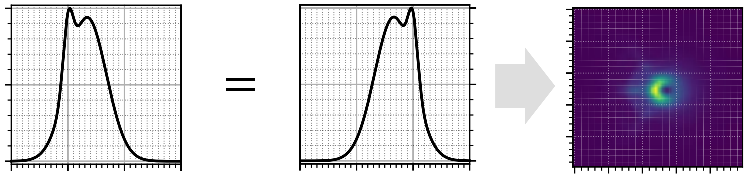

1. Find centroid and set as centre of signal (pad left and right accordingly).
2. Check orientation with skewness and flip to make it always positive (≥ 0).

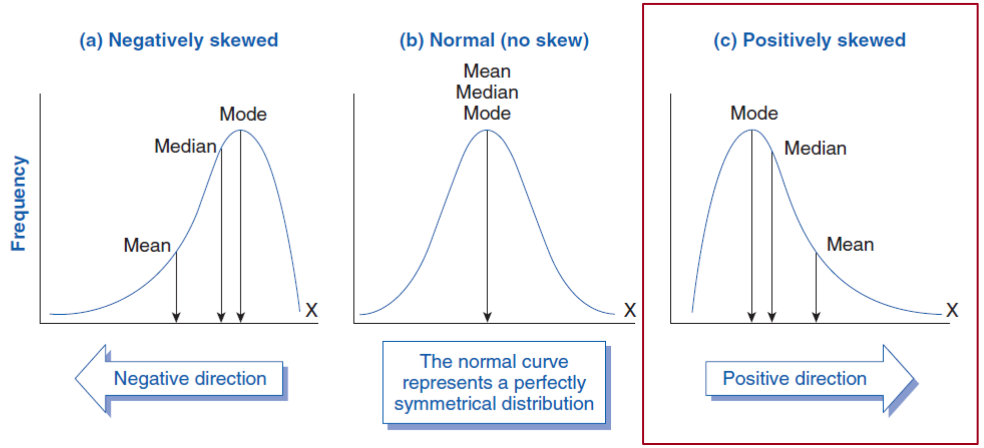

https://www.biologyforlife.com/skew.html

Figure 20. Ready-for-training bunch profile.

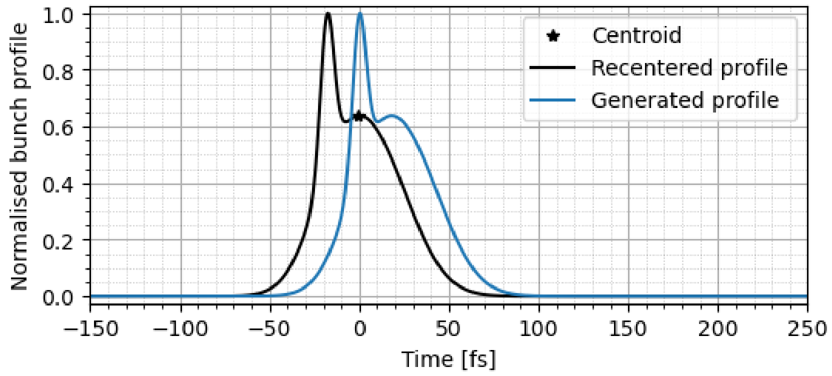

5. Longitudinal profile reconstruction

Phase 1: Pre-processing results

Example shots:

Figure 21. Example of 1D scan for TDC reference profiles and CTR images.

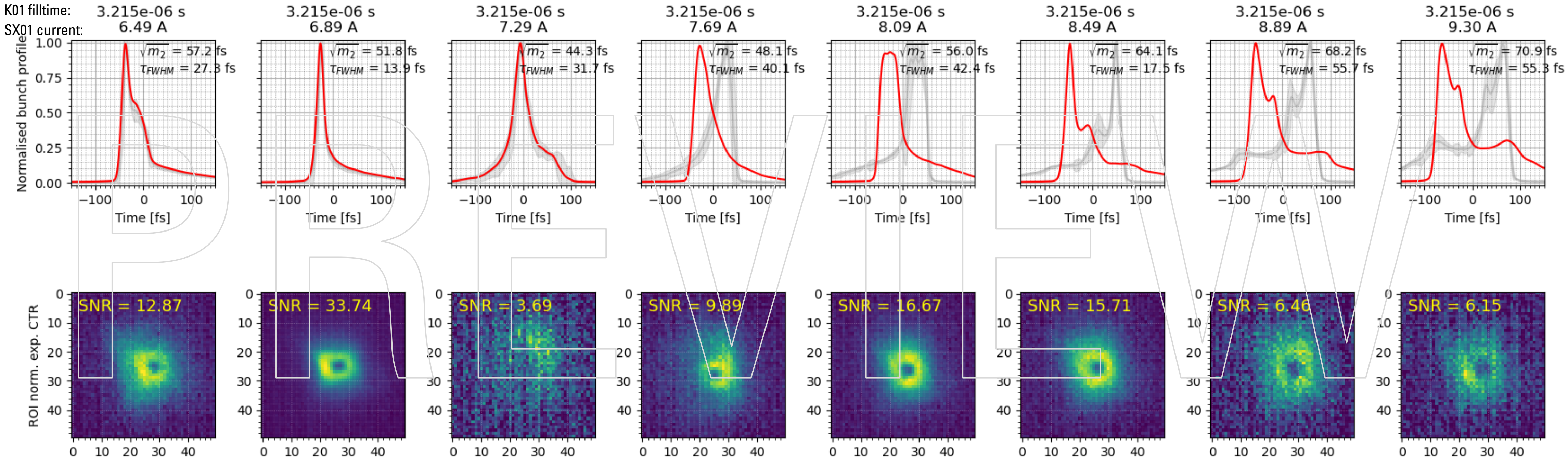

SNR: Signal-to-noise ratio (worse/lower at longer wavelengths = longer features in the profiles)

5. Longitudinal profile reconstruction

Phase 2: Training on experimental data, ***testing in single-shot mode***

› Training on multiple CTR shots per average profile.

Training	100 (15%) x 20 shots (for jitter)	= 2000 samples
Testing	571 (85%) x 1 shot (single shot)	= 571 samples

Metric	**Percentage**
$R^2 > 0.80$	477/571 (~81%)
$R^2 > 0.95$	250/571 (~41%)

Figure 22. R^2 metric for single-shot reconstructions.

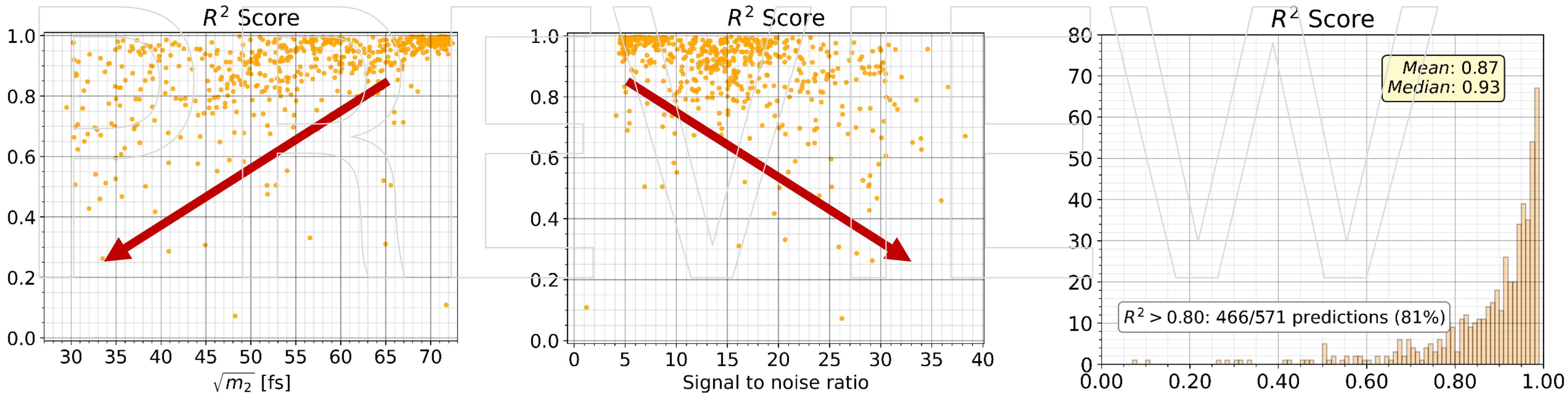

A.M.Guisao-Betancur@liverpool.ac.uk

5. Longitudinal profile reconstruction

*Phase 2: Training on experimental data, **testing multi-shot statistics***

- Training on multiple CTR shots per average profile.
- Testing the statistics by testing on several consecutive shots.

Training	100 (15%) x 20 shots (for jitter)	= 2000 samples
Testing	571 (85%) x 20 shots (multi-shot)	= 571 samples

Metric	Percentage	
$R^2 > 0.80$	532/571 (~92%)	+11%
$R^2 > 0.95$	277/571 (~49%)	+8%

In comparison to single-shot statistics

Figure 23. R^2 metric for single-shot reconstructions averaged over 20 shots.

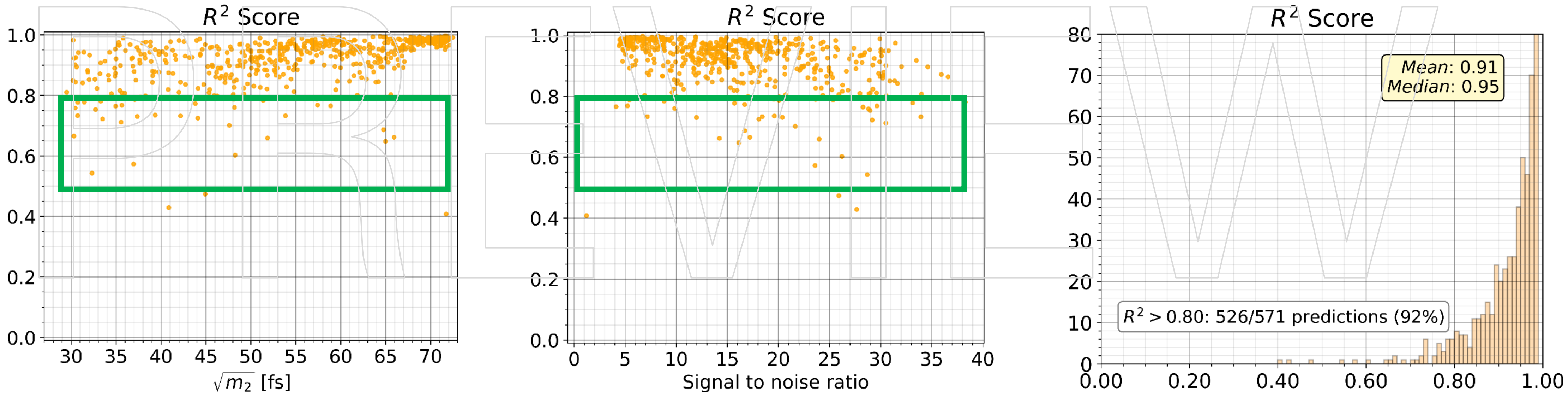

A.M.Guisao-Betancur@liverpool.ac.uk

5. Longitudinal profile reconstruction

*Phase 2: Training on experimental data, **testing multi-shot statistics***

1D Scan: Filltime: 1 step
Current: 61 steps

From the TDC reference

Reconstruction results

Figure 24. R^2 metric for single-shot reconstructions discriminated by current.

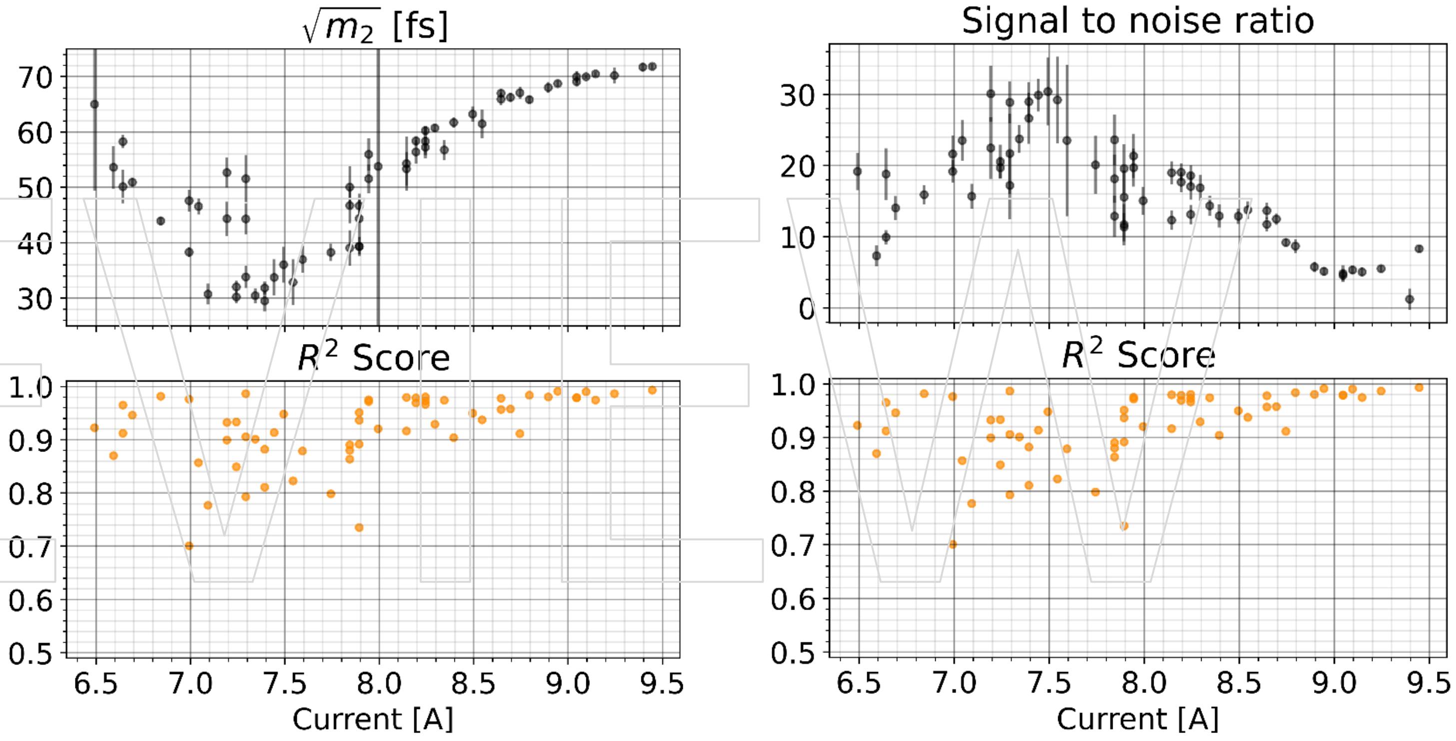

More sensitivity to jitter at high compression

6. Discussion and conclusions

A.M.Guisao-Betancur@liverpool.ac.uk

6. Discussion and conclusions

1 Compact design.

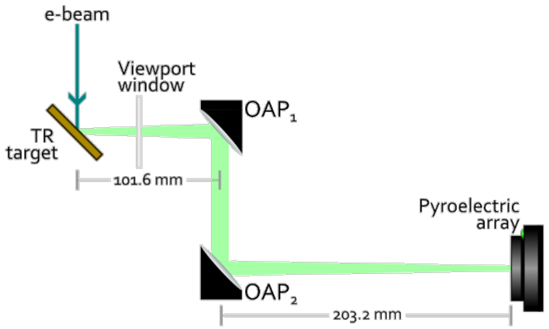

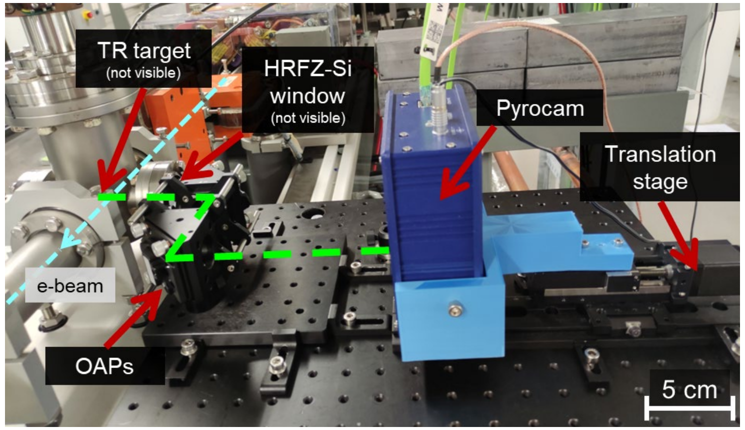

2 Femtosecond range bunch profile reconstruction.

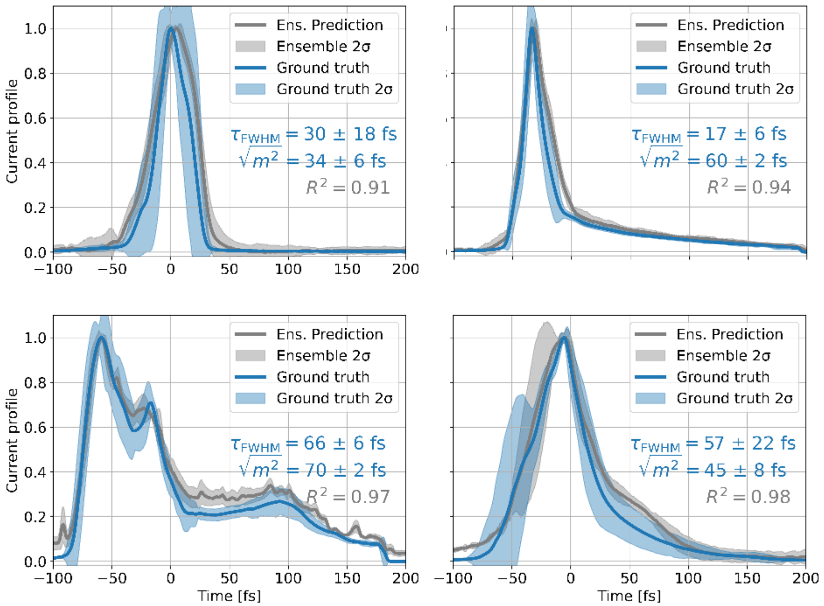

Over a wide range of machine parameters

3 Transfer the technology:

another short-pulse accelerator.

Conventional or plasma-based

Expand and/or shift the bandwidth. → Higher resolution (towards sub-fs) moving from THz to VIS-IR range.

6. Discussion and conclusions

④ Online operation.

CTR images' location

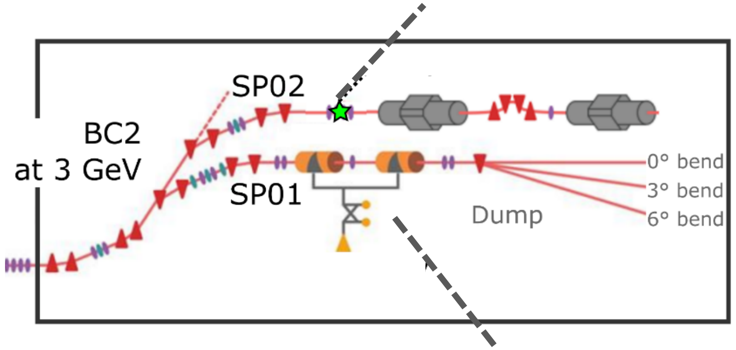

Transverse deflecting cavity (TDC) for reference measurements

About reliable measurements:

- **It needs a reference for training**: from TDC measurements or realistic simulations.
- **It needs periodic re-training:** to remove the effects of drift.
- **It needs enough data to model noise:** more data helps minimise the effects of jitter.

About invasiveness:

- **While operating with transition radiation:**
  - On the current design: an actuator on the target **can be placed only when needed.**
  - When designing from zero: with knowledge of the bunch length ranges a design using a foil would introduce minimum beam scatter.

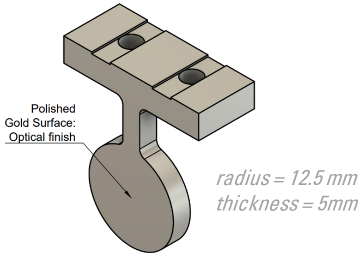

- **Extending to minimally-invasive sources of coherent radiation:** such as the non-intercepting coherent diffraction or synchrotron radiation.

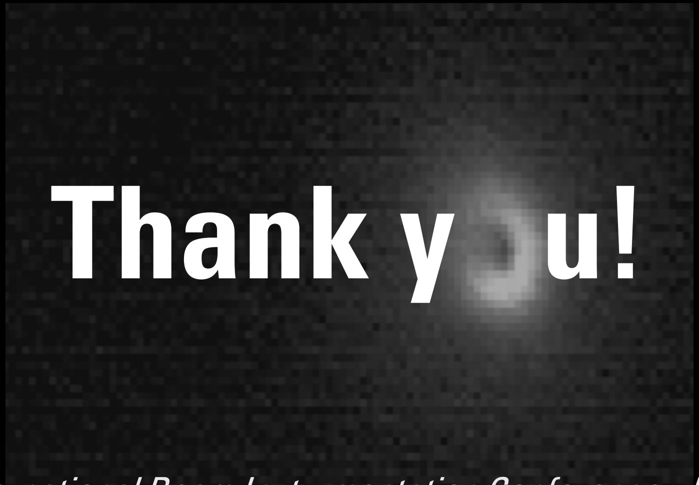

15th International Beam Instrumentation Conference - IBIC 2026

September 1st, 2026

Ana Guisao-Betancur[1,2], Joseph Wolfenden[1,2], Erik Mansten[3], Sara Thorin[3], Johan Lundquist[4], Oliver Grimm[3], Carsten Welsch[1,2]

A.M.Guisao-Betancur@liverpool.ac.uk

[1]. Department of Physics, University of Liverpool, Liverpool L69 7ZX, UK
[2]. Cockcroft Institute, Sci-Tech Daresbury, Daresbury WA4 4AD, UK
[3]. MAX IV Laboratory, Lund University, Lund 224 84, Sweden
[4]. Department of Physics, Lund University, Lund 223 64, Sweden

EuPRAXIA Doctoral Network

UNIVERSITY OF LIVERPOOL

QUASAR GROUP

The Cockcroft Institute of Accelerator Science and Technology

References

1. M. C. Downer, R. Zgadzaj, A. Debus, U. Schramm, and M. C. Kaluza, "Diagnostics for plasma-based electron accelerators", Rev. Mod. Phys., vol. 90, no. 3, p. 035002, 2018. doi:10.1103/RevModPhys.90.035002
2. A. Cianchi et al., "Frontiers of beam diagnostics in plasma accelerators", in Proc. LINAC'18, Beijing, China, Sep. 2018, pp. 977-981. doi:10.18429/JACoW-LINAC2018-FR1A03
3. C. Behrens et al., "Few-femtosecond time-resolved measurements of X-ray free-electron lasers", Nat. Commun., vol. 5, p. 3762, 2014. doi:10.1038/ncomms4762
4. E. Prat et al., "Experimental characterization of the optical klystron effect to measure the intrinsic energy spread of highbrightness electron beams", Phys. Rev. Accel. Beams, vol. 27, no. 3, p. 030701, 2024. doi:10.1103/PhysRevAccelBeams.27.030701
5. E. Prat et al., "Attosecond time-resolved measurements of electron and photon beams with a variable polarization Xband radiofrequency deflector at an X-ray free-electron laser", Adv. Photonics, vol. 7, no. 2, p. 026002, 2025. doi:10.1117/1.AP.7.2.026002
6. A. G. Shkvarunets and R. B. Fiorito, "Vector electromagnetic theory of transition and diffraction radiation with application to the measurement of longitudinal bunch size", Phys. Rev. ST Accel. Beams, vol. 11, no. 1, p. 012801, 2008. doi:10.1103/PhysRevSTAB.11.012801
7. D. V. Karlovets and A. P. Potylitsyn, "Universal description for different types of polarization radiation", 2009. arXiv:0908.2336
8. A. Gillespie, "Bunch length diagnostics: current status and future directions", in Proc. CERN Accelerator School: Beam Instrumentation, Tuusula, Finland, Jun. 2018, pp. 314-363. CERN-ACC-2020-0010.
9. B. Schmidt et al., "Longitudinal bunch diagnostics using coherent transition radiation spectroscopy", 2018. arXiv:1803.00608
10. O. Zarini et al., "Multioctave high-dynamic range optical spectrometer for single-pulse, longitudinal characterization of ultrashort electron bunches", Phys. Rev. Accel. Beams, vol. 25, no. 1, p. 012801, 2022. doi:10.1103/PhysRevAccelBeams.25.012801
11. I. V. Konoplev, G. Doucas, H. Harrison, A. J. Lancaster, and H. Zhang, "Single shot, nondestructive monitor for longitudinal subpicosecond bunch profile measurements with femtosecond resolution", Phys. Rev. Accel. Beams, vol. 24, no. 2, p. 022801, 2021. doi:10.1103/PhysRevAccelBeams.24.022801
12. H. Yamada et al., "Study of coherent Smith-Purcell radiation in the terahertz region using ultra-short electron bunches", Particles, vol. 6, no. 3, pp. 693-702, 2023. doi:10.3390/particles6030042
13. A. Curcio et al., "Noninvasive bunch length measurements exploiting Cherenkov diffraction radiation", Phys. Rev. Accel. Beams, vol. 23, no. 2, p. 022802, 2020. doi:10.1103/PhysRevAccelBeams.23.022802
14. S. Stuchebrov et al., "Coherent Cherenkov diffraction radiation in super-radiant regime as a tool for longitudinal diagnostics", Radiat. Phys. Chem., vol. 240, p. 113415, 2025. doi:10.1016/j.radphyschem.2025.113415
15. T. J. Maxwell et al., "Coherent-radiation spectroscopy of fewfemtosecond electron bunches using a middle-infrared prism spectrometer", Phys. Rev. Lett., vol. 111, no. 18, p. 184801, 2013. doi:10.1103/PhysRevLett.111.184801
16. J. Wolfenden, C. P. Welsch, T. H. Pacey, and A. Shkvarunets, "Coherent transition radiation spatial imaging as a bunch length monitor", in Proc. IPAC'19, Melbourne, Australia, May 2019, pp. 2713-2716. doi:10.18429/JACoW-IPAC2019-WEPGW095
17. M. Castellano, A. Cianchi, G. Orlandi, and V. A. Verzilov, "Effects of diffraction and target finite size on coherent transition radiation spectra in bunch length measurements", Nucl. Instrum. Methods Phys. Res. A, vol. 435, no. 3, pp. 297-307, 1999.doi:10.1016/S0168-9002(99)00566-5
18. A. Guisao-Betancur et al., "Designing a femtosecondresolution bunch length monitor using coherent transition radiation images", Instruments, vol. 9, no. 4, p. 29, 2025. doi:10.3390/instruments9040029
19. A. Guisao-Betancur, C. Welsch, and J. Wolfenden, "Studying Coherent Transition Radiation Spatial Image Features for Bunch Length Diagnostics", presented at the IPAC'26, Deauville, France, May 2026, paper WEP6087, unpublished.
20. A. Guisao-Betancur et al., "Single-shot electron bunch profile monitor based on coherent transition radiation imaging", in Proc. IBIC'25, Liverpool, UK, Sep. 2025, pp. 608-610. doi:10.18429/JACoW-IBIC2025-WEPC001
21. O. Convery, L. Smith, Y. Gal, and A. Hanuka, "Uncertainty quantification for virtual diagnostic of particle accelerators", Phys. Rev. Accel. Beams, vol. 24, no. 7, p. 074602, 2021. doi:10.1103/PhysRevAccelBeams.24.074602